Research Article

Comparative Performance of Label-Free HER2 Immunosensors on Bare, Poly(P-Anisidine)-Modified, and Ammonium Alginate-WO_3-Modified Glassy Carbon Electrodes

Mohammed N. Alabbasi[1,*], Amer Th. Al-Taee[2], and Luay A. Al-Helaly[2]

[1] Department of Chemistry, College of Education for Women, University of Mosul, Mosul, Iraq
[2] Department of Chemistry, College of Science, University of Mosul, Mosul, Iraq
*Corresponding author: Mohammed Nayef Alabbasi
E-mail: mohammed.nayef@uomosul.edu.iq

Abstract

The transducer architecture of a label-free electrochemical immunosensor can alter signal transport, calibration shape, and short-term stability, but these effects are not necessarily aligned. This study compared three glassy-carbon platforms for detection of the extracellular domain of human epidermal growth factor receptor 2 (HER2-ECD): activated bare glassy carbon (GCE), poly(p-anisidine)-modified GCE (GCE/PPA), and GCE/PPA coated with an ammonium alginate-tungsten trioxide nanocomposite [GCE/PPA/(AmAlg-WO_3)]. Each platform was combined with trastuzumab (Ab_T), pertuzumab (Ab_P), or an equal-mass trastuzumab-pertuzumab mixture (Ab_{TP}), producing nine independently calibrated immunosensors. PPA electropolymerization was optimized over 6-15 cyclic-voltammetric cycles; 10 cycles gave the largest charge (72.1 µC). Ferri/ferrocyanide differential-pulse voltammetry was used only to compare electrode architectures. Relative to bare GCE, signal retention decreased to 51.9% after PPA deposition and recovered to 70.7% after AmAlg-WO_3 coating. HER2 measurements were then performed without ferri/ferrocyanide by following the decrease in the approximately 0.9 V peak observed after EDC/NHS treatment. Cumulative HER2 additions covered 1.99-195 ng mL^{-1}, and response was defined as $\Delta I = I_0 - I_{HER2}$. All configurations followed a baseline-adjusted saturation model, with R^2 values of 0.9942-0.9998. Model-derived detection and quantification limits ranged from 0.052 to 0.286 ng mL^{-1} and from 0.158 to 0.911 ng mL^{-1}, respectively. GCE/Ab_{TP} produced the smallest calibration errors (RMSE 0.0697 µA; MAE 0.0593 µA) and the lowest calculated detection limit (0.052 ng mL^{-1}), whereas GCE/PPA/(AmAlg-WO_3)/Ab_{TP} showed the smallest 45-min drift (0.92%). Thus, the bare mixed-antibody sensor provided the strongest calibration performance, while the nanocomposite mixed-antibody sensor provided the best short-term operational stability. The results show that increased absolute current or interfacial transport does not alone determine analytical quality and that architecture should be selected against the intended performance criterion.

Keywords: HER2-ECD; label-free immunosensor; glassy carbon electrode; poly(p-anisidine); tungsten trioxide; differential pulse voltammetry.

1. Introduction

The protein target for the measurement of HER2-ECD is chemically sophisticated because it necessitates selective recognition within a concentration band applicable for the diagnosis of breast cancer—which reduces the signal loses arising from the matrix effects. The use of electrochemical immunosensors is a convenient option for this task, as the association of the binding of antibodies with a small-size electrical transducer allows for the reading of data without using optical instruments typical of conventional immunoassays. However, reviews on electrochemical cancer biosensor technologies note that the validity is determined not only by the recognition element, but by all elements forming the whole interface: electrode materials, the functional layer, immobilization chemistry, redox reaction, and data model [1–3].

HER2 sensors published have demonstrated numerous methods to increase surface area or to enhance signal including bioconjugates of iron oxide, gold and carbon nanostructures, labels of quantum dots, surfaces of hydrogel and immunoassays of a sandwich format [4–7]. Though these methods can provide low limits of detection, they may also lead to further steps of preparation, labels or materials used, which create difficulties for the comparison of the transducer and the antibody layer. Meanwhile, label-free methods have a complementary way whereby some electrochemical signal changes in the time when the binding event happens, however, the mechanism of the step of interface that dictates the observed response has to be correctly inferred in this case [8–9].

Glassy carbon acts as a beneficial base electrode due to its ability to be polished, electrically activated, and optimized. The introduction of the films of conductive or semiconducting polymers may help with the attachment of biomolecules to the electrode; however, the film growth may also prevent charge transfer from occurring.

Electrochemical research on poly(furfurylamine) and hybrids showed that the modification could affect the accessibility of peaks from the electrodes [10–12]. Poly(p-anisidine) is affected in a similar way [13]. The application of polysaccharide-metal-oxide composites could recover the transport loses occurring in the polymer film and provide a biocompatible matrix for the subsequent bioconjugation. Nanocomposites with WO_3 were studied regarding their usage in electrochemical sensing, but their usage does not guarantee the precision of measurements [14].

Another design variable is the antibody system. While trastuzumab binds with domain IV of HER2's extracellular part, pertuzumab attaches to domain II of the same structure [15–16]. Therefore, using both antibodies together allows for binding to two different regions. The extent to which this structural complementarity affects the performance of the analysis depends on the loading of the surface, orientation, accessibility, and signal transduction pathway. Since the presence of the attached antibody can have an impact on the availability of the active site, the question of such an effect should be answered through the experimental results, rather than only taking into account the difference in binding locations [17–18].

The current research was created with the purpose of separating these combined influences into one testing environment. Three electrode setups-bare GCE, GCE/PPA, and GCE/PPA/(AmAlg-WO_3)-were tested with trastuzumab, pertuzumab, and a mixed sample with total amount of material equal to other experiments carried out. The main target was to compare (i) performance of the electrodes in functional charge transportation, (ii) nonlinear calibrating capacity of immunosensors for the measurement of HER2 level, and (iii) short-term operational stability. Data concerning serum response and ELISA comparison were not considered in this paper but will appear in another paper of paired clinical study.

2. Materials and Methods

2.1 Reagents and electrochemical system

Electrochemical measurements were made with a Metrohm 797 VA Computrace using a three-electrode cell. A 3 mm glassy-carbon disk served as the working electrode, Ag/AgCl as the reference electrode, and platinum as the auxiliary electrode. The principal reagents were p-anisidine (≥99%), ammonium alginate, WO_3 nanoparticles (99.9%, <100 nm), EDC hydrochloride, NHS, bovine serum albumin (BSA), potassium ferricyanide, potassium ferrocyanide trihydrate, potassium chloride, and 0.3 µm alumina polishing powder. Recombinant human HER2-ECD (Met1-Thr652, C-terminal His tag; Sino Biological, Cat. No. 10004-H08H) was used as the calibration protein. Trastuzumab was prepared from Herceptin and pertuzumab from Perjeta.

Phosphate buffer was prepared at 0.1 mol L^{-1} total phosphate and pH 7.40 from KH_2PO_4 and K_2HPO_4 without added NaCl or KCl. The ferri/ferrocyanide architecture-evaluation solution contained 5 mmol L^{-1} $K_3[Fe(CN)_6]$, 5 mmol L^{-1} $K_4[Fe(CN)_6]\cdot 3H_2O$, and 0.100 mol L^{-1} KCl. This probe was used only to compare the three electrode surfaces near 0.2 V and was not present during HER2 calibration.

2.2 Electrode cleaning, activation, and PPA electropolymerization

The GCE surface was rinsed with distilled water and polished for approximately 10 s on a clean cloth with 0.3 µm Al_2O_3 using light, regular motion. The electrode was then ultrasonicated in ethanol and distilled water for 5 min in each liquid. Electrochemical activation was performed in 10 mL of an aqueous acid mixture containing approximately 0.0552 mol L^{-1} H_2SO_4 and 0.0158 mol L^{-1} HNO_3. Five CV sweeps were applied from 0.00 to +1.20 V at 1.0 V s^{-1} with a 0.006 V step. After activation, the electrode and cell were rinsed with water and PBS.

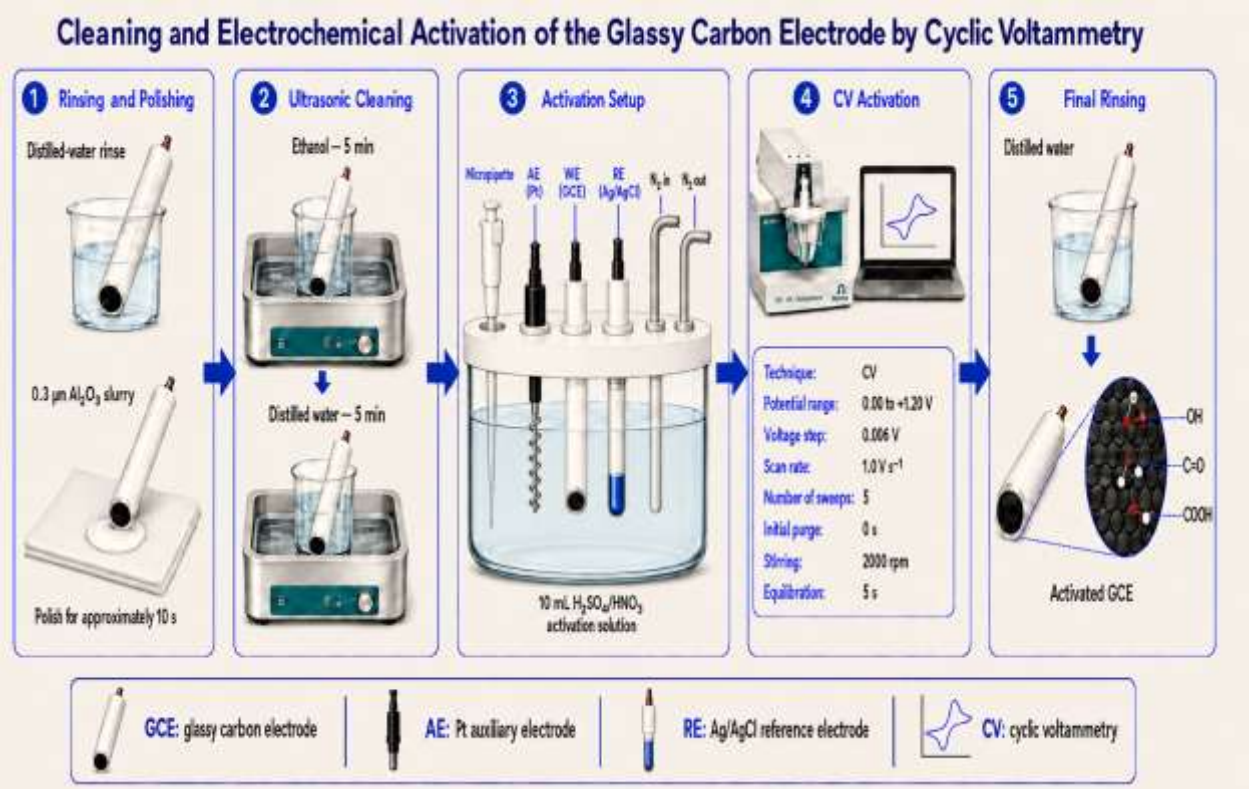

Figure 1. Cleaning, polishing, and electrochemical activation of the glassy carbon electrode using cyclic voltammetry.

The PPA solution contained 0.01 mol L^{-1} p-anisidine, 0.1 mol L^{-1} KCl, and 0.5 mol L^{-1} H_3PO_4. Electropolymerization was conducted between -0.30 and +1.30 V at 0.050 V s^{-1} with a 0.006 V step. The effect of cycle number was evaluated from 6 to 15 cycles. Charge extracted from the resulting voltammograms was used as the operational criterion for selecting the polymerization condition; 10 cycles were then used for all GCE/PPA and GCE/PPA/(AmAlg-WO_3) electrodes.

2.3 Construction and functional evaluation of the three electrode architectures

The first architecture was the cleaned and activated GCE. The second was formed by electropolymerizing PPA on the activated surface. For the third, ammonium alginate (1.0 mg mL^{-1}) and WO_3 nanoparticles (2.0 mg mL^{-1}) were dispersed in deionized water by stirring and ultrasonication. A 10 µL aliquot was drop-cast onto GCE/PPA, delivering 10 µg ammonium alginate and 20 µg WO_3, and was allowed to dry completely before gentle PBS washing.

Functional charge transport was compared by DPV in the ferri/ferrocyanide solution. The evaluation scan extended from -0.30 to +0.80 V with a +0.10 V pulse amplitude, 0.010 s pulse time, 0.005 V step, and 0.40 s step time. The resulting charge was summarized as a midpoint between the recorded minimum and maximum values. Signal retention was estimated concerning bare GCE, and calculated apparent blocking was estimated as 100% minus retention. These indicators indicate the functional effect of each coating over the reaction of the probe; they do not measure the thickness of the film, distribution of the particles or size of the electroactive area.

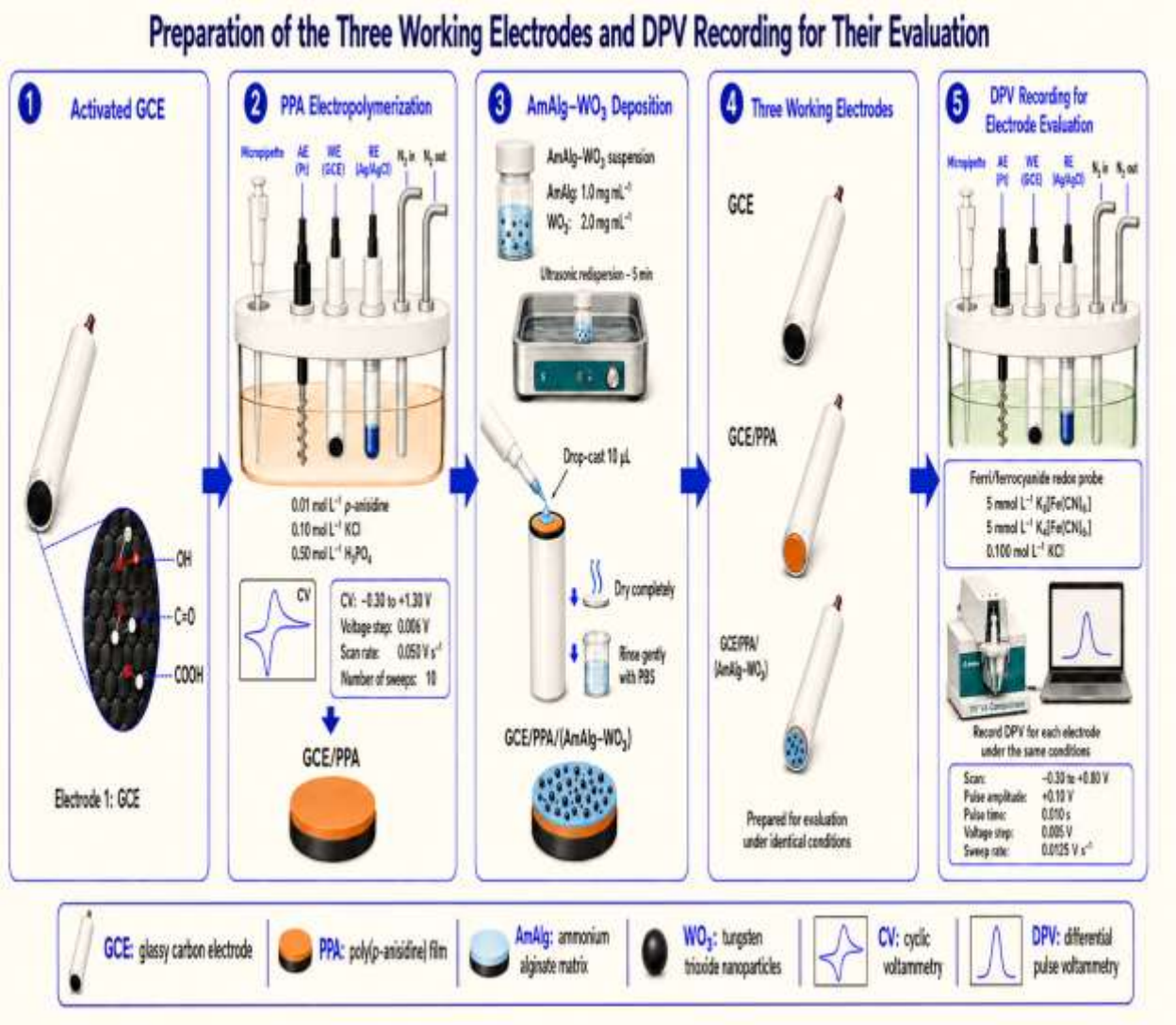

Figure 2. Preparation of the GCE, GCE/PPA, and GCE/PPA/(AmAlg-WO_3) working electrodes and their electrochemical evaluation by differential pulse voltammetry.

2.4 Antibody immobilization and immunosensor assembly

EDC·HCl and NHS were freshly prepared in cold PBS at 0.5 mol L^{-1}. In the electrochemical cell, 10 µL EDC solution and 10 µL NHS solution were added sequentially to 5.00 mL PBS. After surface activation, the electrode was removed and positioned with the disk facing upward. Trastuzumab or pertuzumab was immobilized by applying 10 µL of a 50 µg mL^{-1} solution, corresponding to 0.50 µg antibody. The mixed system contained 5 µL trastuzumab plus 5 µL pertuzumab at the same working concentrations, corresponding to 0.25 µg of each antibody and the same total antibody mass (0.50 µg) used for the single-antibody systems. Immobilization proceeded for 40 min in a cooled humid chamber, followed by gentle PBS washing. A 10 µL aliquot of 0.1% (w/v) BSA was then applied for 20 min to block remaining nonspecific sites. After washing, the sensor was returned to the cell and its initial peak current, I_0, was recorded.

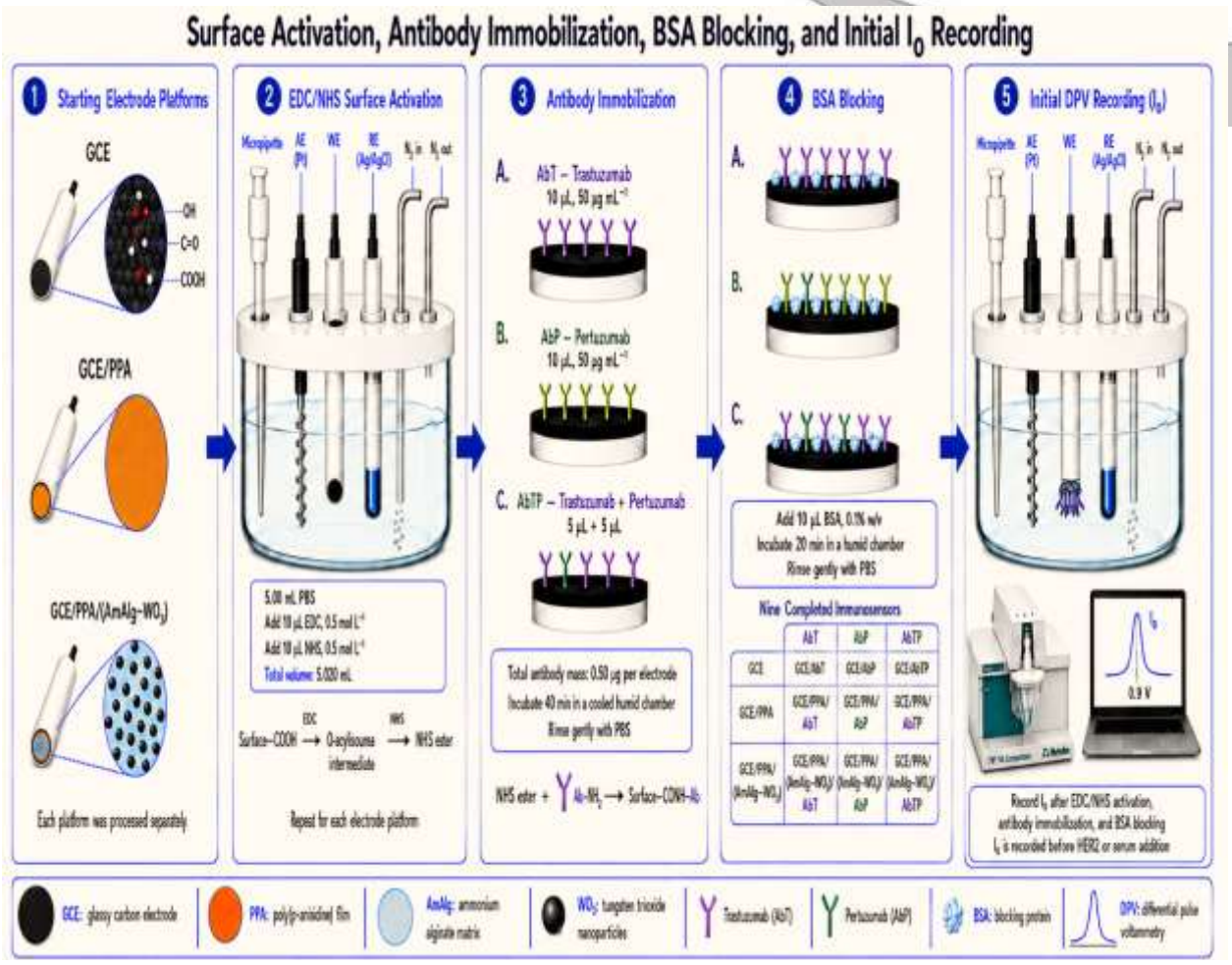

Figure 3. Construction of the label-free HER2 immunosensors through EDC/NHS surface activation, immobilization of trastuzumab, pertuzumab, or their mixture, BSA blocking, and recording of the initial current (I_0).
Crossing the three electrodes with the three recognition systems generated nine sensors: GCE/Ab_T, GCE/Ab_P, GCE/Ab_{TP}, GCE/PPA/Ab_T, GCE/PPA/Ab_P, GCE/PPA/Ab_{TP}, GCE/PPA/(AmAlg-WO_3)/Ab_T, GCE/PPA/(AmAlg-WO_3)/Ab_P, and GCE/PPA/(AmAlg-WO_3)/Ab_{TP}.

2.5 HER2 calibration and signal definition

Each immunosensor was calibrated independently by cumulative addition of HER2 working solution to the same cell. Before the first addition, the cell volume was 5.020 mL (5.00 mL PBS plus 10 µL EDC and 10 µL NHS). Additions were selected to produce final HER2 concentrations of 1.99, 5.97, 9.95, 13.9, 19.9, 29.8, 39.7, 69.2, 98.6, 147, and 195 ng mL^{-1} after correction for the increasing volume. A 5 min waiting period followed every addition before DPV acquisition.

HER2 measurements did not use ferri/ferrocyanide. Instead, the analytical signal was the decrease in the peak near 0.9 V that appeared after addition of the EDC/NHS reagents. This feature was treated operationally as an EDC/NHS-associated peak and not as an established redox signal of HER2 itself. The response was calculated from the blocked, antibody-bearing sensor current before HER2 exposure and the current after binding:

$\Delta I = I_0 - I_{HER2}$ (1)

For the GCE, GCE/PPA, and GCE/PPA/(AmAlg-WO_3) immunosensors, the DPV scan extended from -0.30 to +1.30 V with a +0.10 V pulse amplitude. The respective voltage steps were 0.007, 0.006, and 0.006 V; pulse times were 0.010, 0.020, and 0.020 s; and step times were 0.200, 0.400, and 0.600 s. All curves within a configuration were acquired using the same method file and peak-extraction procedure.

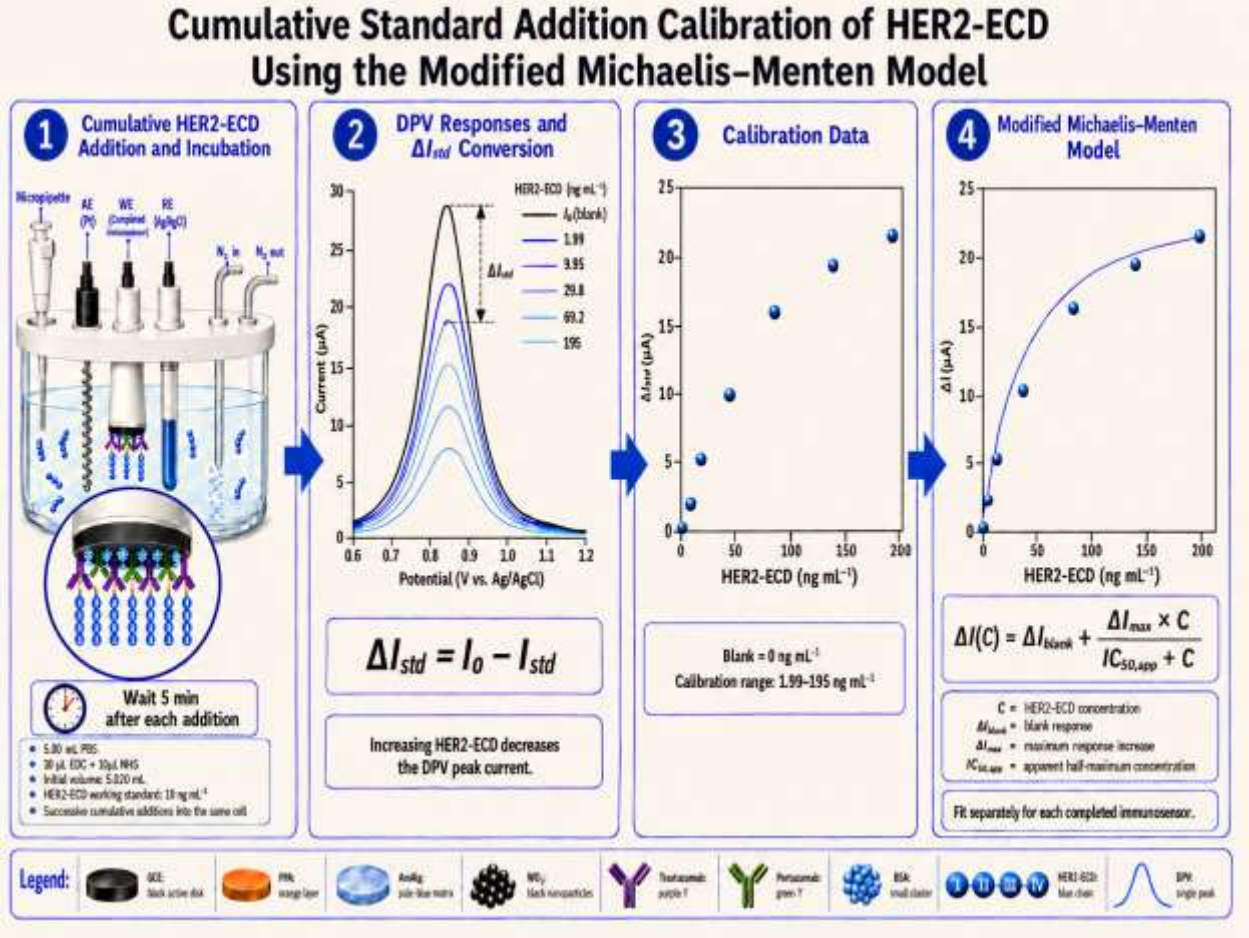

Figure 4. Cumulative standard-addition procedure used for HER2-ECD calibration, including standard addition, a 5 min waiting period, DPV recording, and calculation of the standard response.

2.6 Nonlinear regression and analytical figures of merit

The increasing, saturating concentration-response relation was described with a baseline-adjusted Michaelis-Menten-type equation:

$$\Delta I(C) = \Delta I_{blank} + (\Delta I_{max} \times C)/(IC_{50,app} + C) \quad (2)$$

Here, ΔI_{blank} is the fitted baseline response, ΔI_{max} is the fitted increase above baseline, and $IC_{50,app}$ is the apparent concentration corresponding to half of that increase. The model was selected after comparison with a conventional zero-baseline Michaelis-Menten form and a one-phase exponential association model. Fit quality was assessed with R^2, residual standard error (S), RMSE, MAE, maximum absolute residual, and corrected Akaike information criterion (AIC_c). The initial model slope was calculated as $\Delta I_{max}/IC_{50,app}$. Blank solution was measured three times for each sensor, and its standard deviation (s_{blank}) was used in the model-based limits:

$$LOD = (3.3 \times s_{blank} \times IC_{50,app})/(\Delta I_{max} - 3.3 \times s_{blank}) \quad (3)$$

$$LOQ = (10 \times s_{blank} \times IC_{50,app})/(\Delta I_{max} - 10 \times s_{blank}) \quad (4)$$

Because the resulting limits were below the lowest measured standard, 1.99 ng mL^{-1}, they were interpreted as model-derived estimates rather than directly verified working concentrations.

2.7 Short-term operational stability

Operational stability was evaluated within one measurement session at 0, 5, 10, 15, 30, and 45 min. A single reading was collected at each time for each configuration. Response retention was calculated as $\Delta I(t)/\Delta I(0) \times 100$, and drift as $[\Delta I(t) - \Delta I(0)]/\Delta I(0) \times 100$. The series was therefore interpreted descriptively rather than as replicate stability measurements. A next-day reading obtained while the electrode and immunocomplex remained in the same medium was not used as evidence of storage stability.

3. Results

3.1 Optimization of PPA electropolymerization

The extracted charge changed non-monotonically as the number of CV cycles increased. It rose from 29.7 µC at six cycles to 72.1 µC at ten cycles, then declined to 61.6 µC at eleven cycles and to approximately 7 µC from cycles 12-15. Ten cycles therefore represented the largest measured charge within the tested range and was selected for subsequent electrode preparation.

Table 1. Effect of CV cycle number on PPA electropolymerization charge.

CV cycles	Charge (µC)
6	29.7
7	27.9
8	31.0
9	41.9
10	72.1
11	61.6
12	7.30
13	7.18
14	6.64
15	6.90

Note. Charge was the operational response used to select the polymerization condition. Ten cycles were used for all later PPA-containing electrodes.

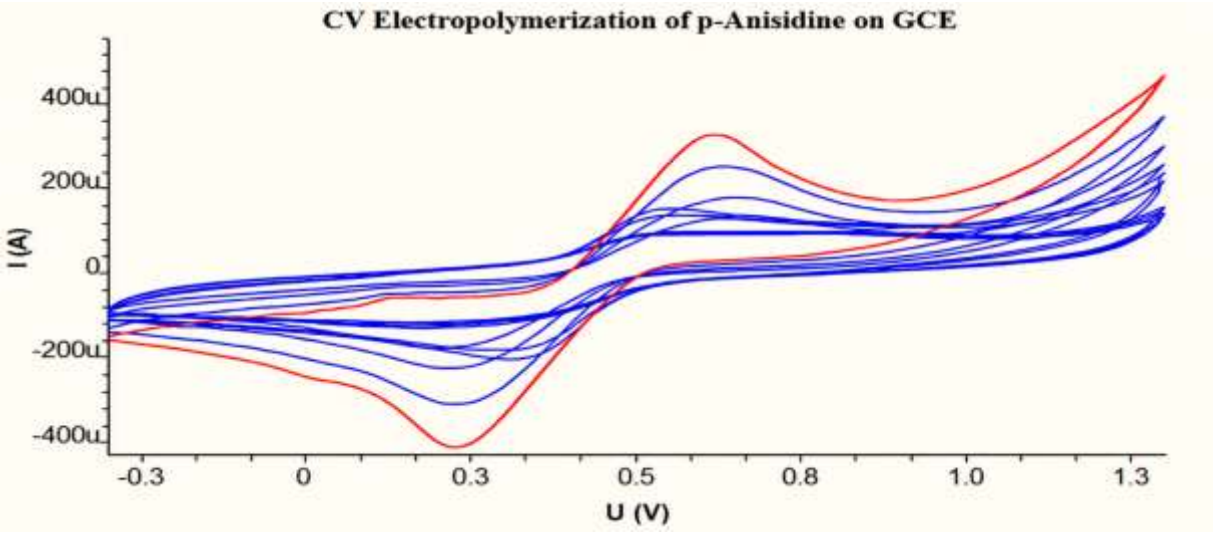

Figure 5. Optimization of p-anisidine electropolymerization from 6 to 15 CV cycles, showing the maximum extracted charge at 10 cycles.

3.2 Functional effect of the sequential electrode modifications

Bare GCE produced a midpoint charge of 2.495 mC in the ferri/ferrocyanide test. PPA deposition reduced the midpoint to 1.295 mC, corresponding to 51.9% retention and 48.1% apparent blocking. Addition of AmAlg-WO_3 increased the midpoint to 1.765 mC, giving 70.7% retention and 29.3% apparent blocking. Thus, the nanocomposite recovered 18.8 percentage points of signal retention relative to GCE/PPA but did not restore the response to the bare-electrode level.

Table 2. Functional comparison of the three electrode architectures using ferri/ferrocyanide DPV.

Architecture	Q_{min} (mC)	Q_{max} (mC)	Q_{mid} (mC)	Retention (%)	Blocking (%)
GCE	2.30	2.69	2.495	100.0	0.0
GCE/PPA	1.25	1.34	1.295	51.9	48.1
GCE/PPA/(AmAlg-WO_3)	1.67	1.86	1.765	70.7	29.3

Note. The ferri/ferrocyanide probe was used only for electrode-architecture evaluation. Retention was calculated relative to GCE.

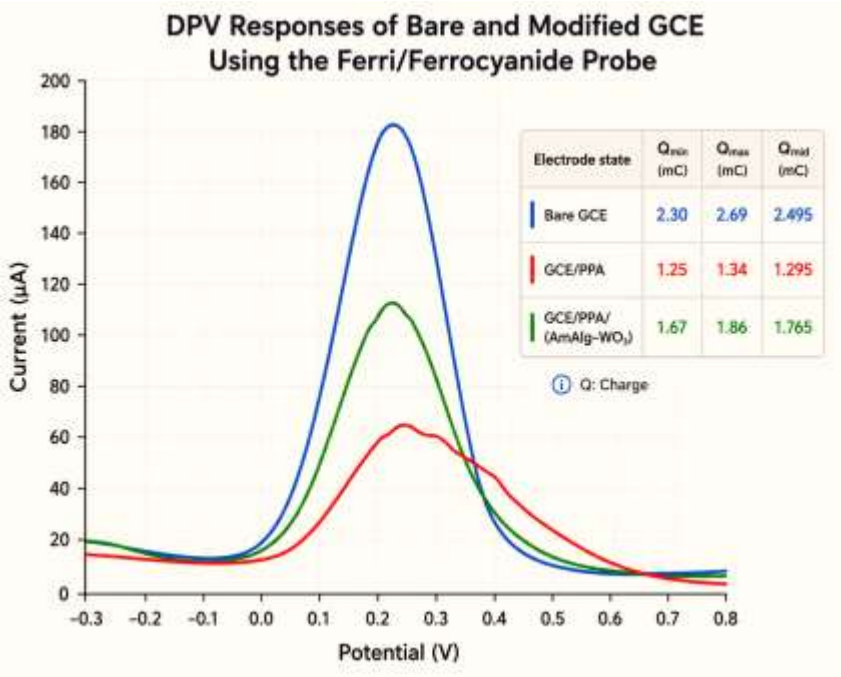

Figure 6. Differential-pulse voltammetric comparison of ferri/ferrocyanide charge transport at GCE, GCE/PPA, and GCE/PPA/(AmAlg-WO_3).

3.3 Nonlinear calibration across the nine immunosensors

All nine configurations showed increasing ΔI with HER2 concentration and approached saturation over 1.99-195 ng mL^{-1}. The fitted baseline-adjusted model described the data with R^2 values between 0.9942 and 0.9998. The bare GCE configurations had the largest fitted response capacities, particularly GCE/Ab_T (ΔI_{max} = 69.43 µA). PPA-containing sensors had smaller fitted maxima (38.17-42.53 µA), whereas addition of AmAlg-WO_3 increased them to 48.72-54.84 µA. This sequence was consistent with the independent ferri/ferrocyanide architecture test: PPA lowered the available electrochemical response, and the nanocomposite partially recovered it.

Precision of calibration is not affected by fitted amplitude only. The model GCE/Ab_{TP} gave the lowest value of RMSE (0.0697 µA), MAE (0.0593 µA), maximum absolute deviation (0.1253 µA), and the most optimal value of the AIC_c (-54.92). The model GCE/Ab_T also fitted well while the two nanocomposite sensors containing the Abs_P or Abs_{TP} had higher residual metrics as they recovered more absolute signal than the respective PPA sensors.

Table 3. Parameters and fit statistics for the baseline-adjusted saturation model.

Configuration	ΔI_{blank}	ΔI_{max}	$IC_{50,app}$	R^2	RMSE	MAE	AIC_c
GCE/Ab_T	2.32	69.43	9.94	0.9996	0.1297	0.1064	-40.02
GCE/Ab_P	1.63	60.27	8.25	0.9986	0.2087	0.1569	-28.60
GCE/Ab_{TP}	1.62	63.31	8.82	0.9998	0.0697	0.0593	-54.92
GCE/PPA/Ab_T	2.65	42.53	13.64	0.9961	0.2505	0.1967	-24.22
GCE/PPA/Ab_P	1.82	38.17	12.21	0.9978	0.1675	0.1537	-33.89
GCE/PPA/Ab_{TP}	2.23	38.80	13.14	0.9975	0.1828	0.1288	-31.78

Configuration	ΔI_{blank}	ΔI_{max}	$IC_{50,app}$	R^2	RMSE	MAE	AIC_c
GCE/PPA/(AmAlg-WO_3)/Ab_T	3.43	54.84	11.82	0.9988	0.1782	0.1269	-32.40
GCE/PPA/(AmAlg-WO_3)/Ab_P	2.12	48.72	9.63	0.9953	0.3139	0.2422	-18.81
GCE/PPA/(AmAlg-WO_3)/Ab_{TP}	2.72	50.46	10.50	0.9942	0.3617	0.2978	-15.41

Note. Current-related parameters and error statistics are in µA; $IC_{50,app}$ is in ng mL^{-1}. The fitted equation was $\Delta I(C) = \Delta I_{blank} + \Delta I_{max}\, C/(IC_{50,app} + C)$.

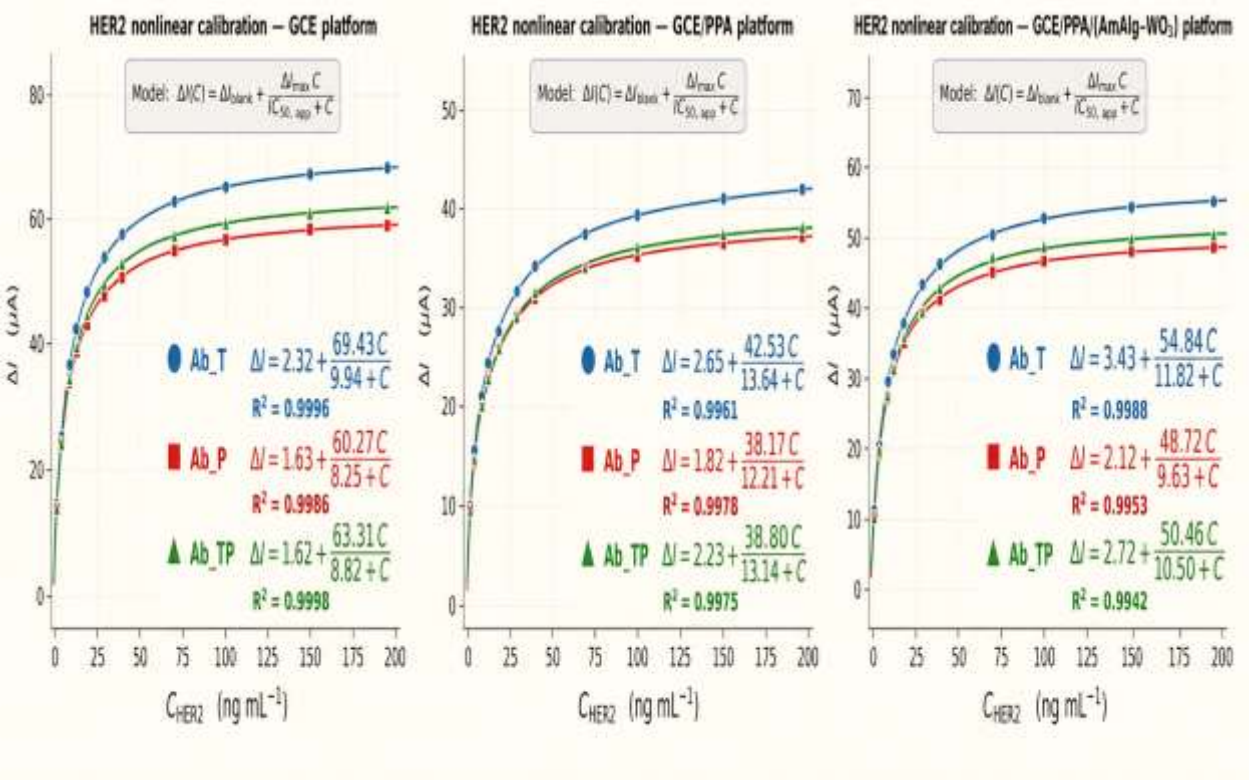

Figure 7. Nonlinear HER2-ECD calibration curves for the nine immunosensors, grouped by GCE, GCE/PPA, and GCE/PPA/(AmAlg-WO_3) architecture.

3.4 Sensitivity and model-derived analytical limits

The initial slopes ranged from 2.953 to 7.305 µA/(ng mL^{-1}). GCE/Ab_P exhibited the highest initial slope (7.305 µA/(ng mL^{-1})), followed by GCE/Ab_{TP} (7.178 µA/(ng mL^{-1})) and GCE/Ab_T (6.985 µA/(ng mL^{-1})). The calculated LOD values varied from 0.052 to 0.286 ng mL^{-1}, and the calculated values of LOQ varied from 0.158 to 0.911 ng mL^{-1}. The lowest values were obtained using GCE/Ab_{TP} (LOD 0.052 ng mL^{-1}; LOQ 0.158 ng mL^{-1}). The mixed-antibody sensors produced lower calculated LOD values within each architecture than the corresponding trastuzumab-only sensors. The nanocomposite Ab_P and Ab_{TP} sensors also produced low calculations although they produced larger residual errors than the GCE/Ab_{TP}.

Table 4. Analytical figures of merit and 45-min operational stability.

Configuration	Sensitivity	LOD	LOQ	Max. residual	Drift (%)	Retention (%)
GCE/Ab_T	6.985	0.121	0.377	0.2986	1.54	101.54
GCE/Ab_P	7.305	0.236	0.759	0.5426	1.76	101.76
GCE/Ab_{TP}	7.178	0.052	0.158	0.1253	4.03	104.03
GCE/PPA/Ab_T	3.118	0.158	0.489	0.4312	4.26	104.26
GCE/PPA/Ab_P	3.126	0.286	0.911	0.2373	1.81	101.81

Configuration	Sensitivity	LOD	LOQ	Max. residual	Drift (%)	Retention (%)
GCE/PPA/Ab_{TP}	2.953	0.092	0.283	0.4814	7.27	107.27
GCE/PPA/(AmAlg-WO_3)/Ab_T	4.640	0.125	0.388	0.3883	4.07	104.07
GCE/PPA/(AmAlg-WO_3)/Ab_P	5.059	0.082	0.254	0.6520	3.04	103.04
GCE/PPA/(AmAlg-WO_3)/Ab_{TP}	4.806	0.087	0.267	0.7236	0.92	100.92

Note. Sensitivity is the initial model slope in µA/(ng mL^{-1}). LOD and LOQ are in ng mL^{-1} and are model-derived from three blank readings per sensor. The measured calibration range for every configuration was 1.99-195 ng mL^{-1}.

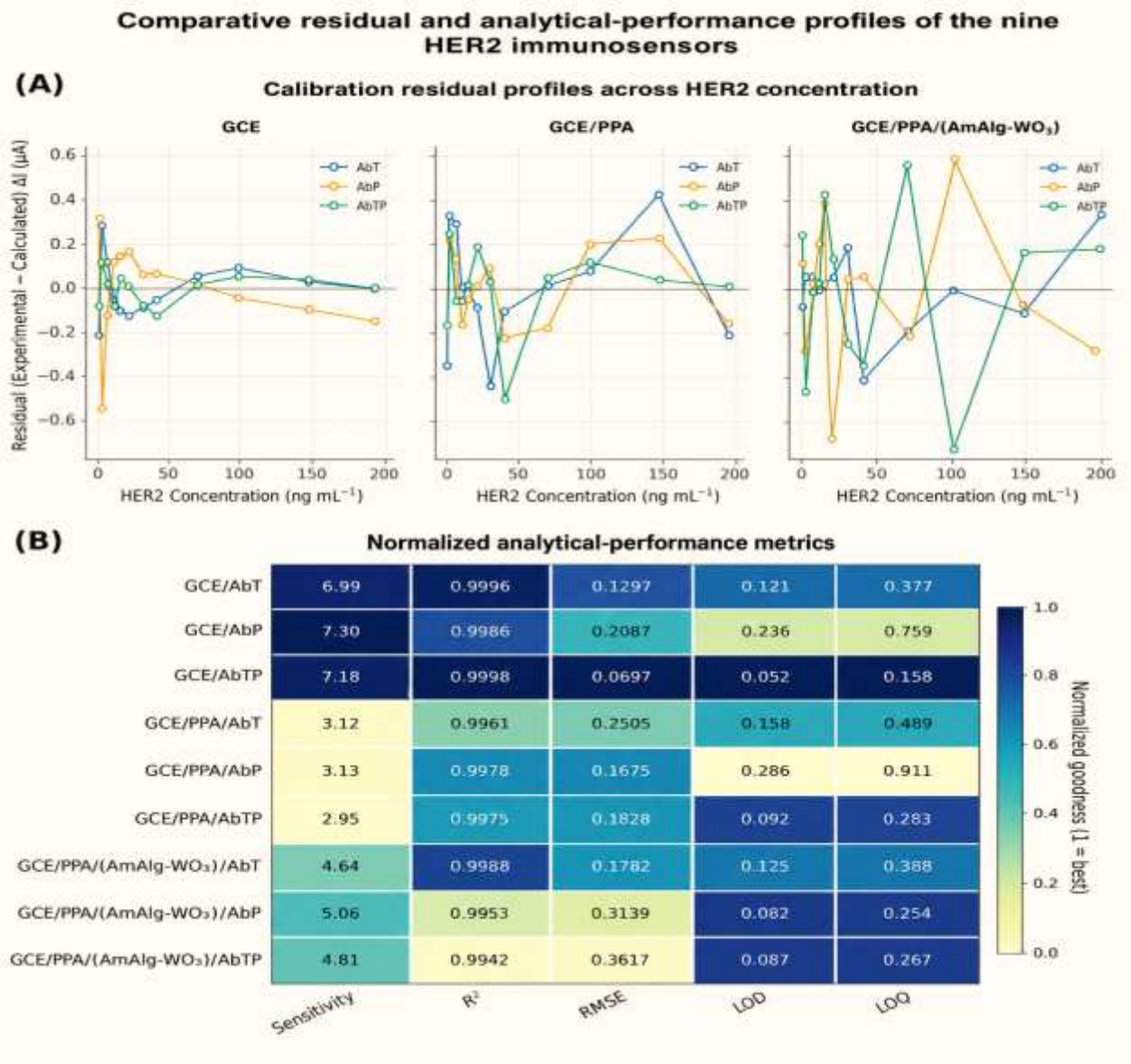

Figure 8. Comparative residual and analytical-performance profiles of the nine HER2 immunosensors.

3.5 Short-term operational stability

The drift readings, at 45 minutes, varied from 0.92 % to 7.27 %. GCE/PPA/(AmAlg-WO_3)/Ab_{TP} is the most stable of the configurations, with a time-zero value of 100.92 %. The GCE/Ab_T, GCE/Ab_P, and GCE/PPA/Ab_P configurations demonstrated drifts of 1.81 % or less. Although GCE/PPA/Ab_{TP} had the highest percent change over the complete

measurement window (7.27 %), it has undergone a change of 0.85 % from the 30- to the 45-minute mark. In contrast, the drifts for the different configurations during the 30- to 45-minute interval were maximum 1.38 %, thereby, proving that 30 min is a reasonable time to take readings at which measurements can reliably be made in later analyses.

The stability ranking differed from the calibration ranking. GCE/Ab_{TP} had the strongest model fit and lowest calculated LOD but drifted by 4.03% over 45 min. Conversely, the nanocomposite mixed-antibody sensor had a somewhat larger calibration residual structure but the smallest temporal drift. No configuration was therefore best on every analytical criterion.

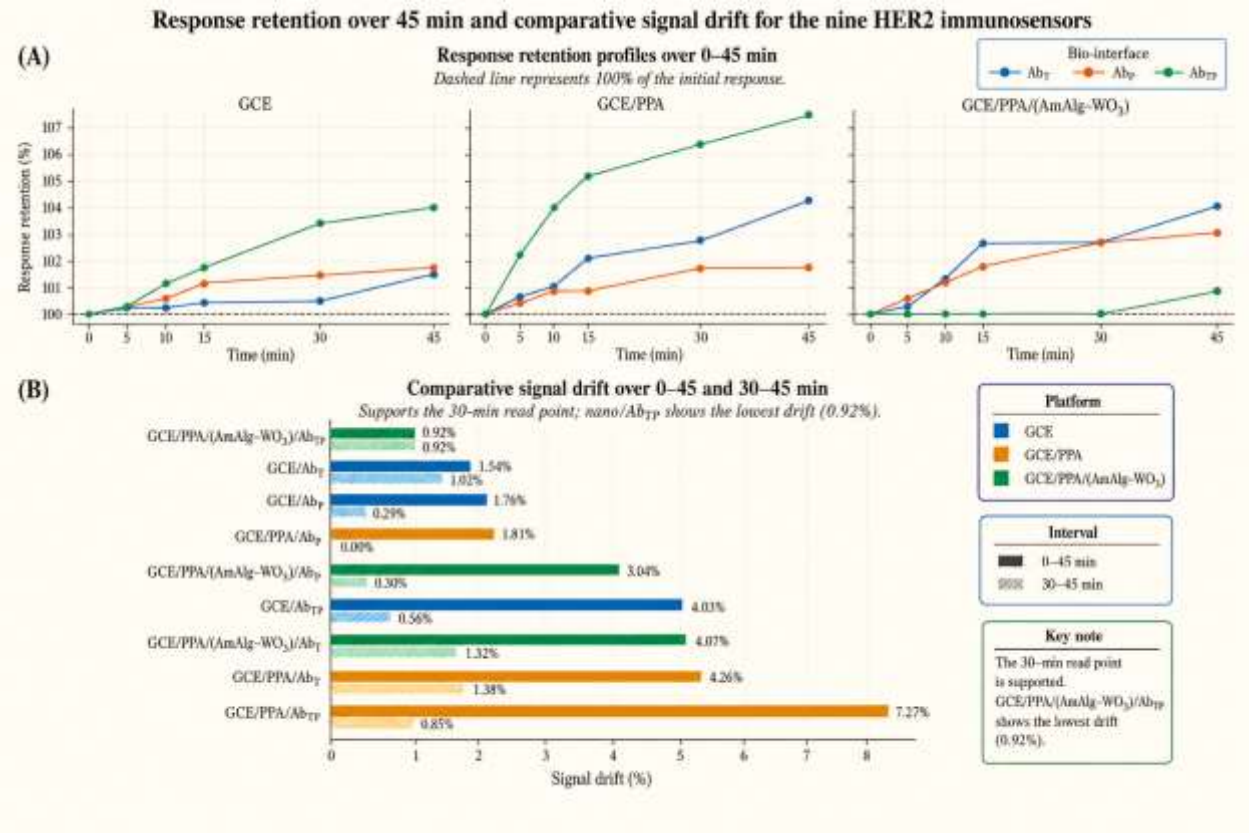

Figure 9. Response retention over 45 min and comparative signal drift for the nine HER2 immunosensors.

4. Discussion

4.1 PPA created a transport barrier, while AmAlg-WO_3 produced partial functional recovery

Observed result. The ferri/ferrocyanide midpoint charge fell from 2.495 mC at bare GCE to 1.295 mC after PPA deposition, then increased to 1.765 mC after application of AmAlg-WO_3. The same order was evident in fitted HER2 response capacity: the bare sensors had the largest ΔI_{max} values, PPA sensors the smallest, and nanocomposite sensors intermediate values.

Interpretation. The decrease after electropolymerization is consistent with the formation of a film that restricts access of the ferri/ferrocyanide couple and alters electron transfer. It should not be interpreted as failure of polymer formation. The abrupt fall in polymerization charge beyond 11 cycles further indicates that increasing cycle count did not continuously improve the electrochemical interface; within the tested conditions, ten cycles gave the best operational balance. The nanocomposite subsequently restored part of the available transport, plausibly by changing the hydrated interfacial pathway and introducing WO_3-containing domains. That interpretation remains functional rather than structural because microscopy, spectroscopy, film-thickness measurements, and electrochemical impedance spectroscopy were not performed.

Relation to previous work. Electropolymerized films are commonly used to introduce functional groups and control surface chemistry, but their influence on peak accessibility depends on thickness and preparation conditions.

Studies of modified carbon electrodes have likewise shown that polymer and polymer-nanomaterial layers can either attenuate or enhance a measured peak according to the charge-transfer pathway and target chemistry [10–12]. WO_3-containing composites have been used to improve biosensor interfaces [14], yet the present data refine that general expectation: AmAlg-WO_3 recovered only part of the signal lost through PPA, and the recovered amplitude did not automatically yield the lowest calibration error.

4.2 Calibration quality depended on architecture and biorecognition together

Observed result. All configurations followed a saturating response, but their fitted parameters and residual metrics differed. GCE/Ab_{TP} was the most precise calibration system by RMSE, MAE, maximum residual, AIC_c, and calculated LOD. GCE/Ab_P had the steepest initial model slope, whereas GCE/Ab_T had the largest fitted response capacity. The nanocomposite increased ΔI_{max} relative to PPA for each antibody condition but did not produce uniformly smaller residuals.

Understanding the findings. The study shows that the sensitivity, amplitude of the probing signal, and accuracy of the model are different characteristics. High ΔI_{max} can strengthen the dynamic signal range, whereas low $IC_{50,app}$ can result in the steep initial angle. Despite this fact, there is no guarantee that the least residuals will be obtained. In the case of GCE/Ab_{TP}, the two sensing elements made the concentration-response curve very consistent on the uncoated activated surface as they were employed at a fixed total mass of 0.50 µg. As a result, the comparison has not been compromised by having had twice as much of antibody immobilized in the mixture being analyzed. The current result can be interpreted as a suggestion that there has been access to domains IV and II, but it does not prove that the receptor was simultaneously occupied or provide information about the orientation of the antibodies on the surface.

Relation to previous work. Structural studies establish that trastuzumab and pertuzumab bind distinct HER2-ECD regions [15–16], providing a rational basis for testing a mixture. Published HER2 electrochemical assays have used a wide range of bioconjugates and signal-amplification formats, including iron-oxide conjugates, quantum-dot labels, and silver-deposition sandwich assays [4–6]. Direct numerical ranking against those studies would be inappropriate because the assay formats, matrices, calibration models, and verification procedures differ. The present contribution is instead an internally controlled comparison of nine label-free configurations prepared and analyzed within one system.

4.3 Interpretation of the EDC/NHS-associated signal

Observed result. HER2 binding was quantified through a decrease in the approximately 0.9 V peak observed after EDC/NHS treatment. Ferri/ferrocyanide was absent from these calibration measurements. The fitted response increased with HER2 concentration because the post-binding current progressively decreased relative to I_0.

Interpretation. The most conservative explanation is that formation of the antibody-HER2 interfacial layer increasingly hindered or altered the process responsible for the EDC/NHS-associated peak. The study did not identify the molecular electrochemical reaction responsible for that feature, and HER2 was not treated as an electroactive species. This distinction prevents conflation of a functional analytical peak with a mechanistically established HER2 redox reaction.

Relation to previous work. Label-free immunosensors frequently translate antigen binding into altered charge transfer, capacitance, impedance, or peak current at a functionalized interface [3,8–9]. EDC/NHS chemistry is widely used to connect carboxyl-bearing surfaces and antibody amino groups, although immobilization orientation and retained binding activity remain important sources of variation [17–18]. The present design used the EDC/NHS-associated feature as an operational signal and therefore requires future mechanistic characterization before stronger electrochemical assignments can be made.

4.4 Model-derived limits require restrained interpretation

Results detected. The calculated limits of detection and quantification (LOD and LOQ) were found to be lower than the minimum calibration standards for the corresponding nine sensors. By using the blank response parameters, the estimates were obtained using data from three blank readings performed for each sensor.

Interpretation. The above values summarize the model and blank variations but do not prove that samples of 0.052-0.911 ng mL^{-1} have been tested or measured with acceptable accuracy and precision. In order to verify, this would require standards generated specifically around the suggested limits, different manufacturing sources for the electrodes and acceptance criteria established beforehand. The working range given could thus be set from 1.99-195 ng mL^{-1}; the lower numbers quoted are still only calculated estimates.

Comparison with earlier studies. Low limits are often highlighted in HER2 biosensor studies and the different approaches to the biosensing of HER2 [4–5,7]. Whenever comparing studies, it should also be determined whether

the limit was taken from measurements, derived from a linear relation, related to a non-linear result, or obtained in a buffer instead of serum. It is important to present the range of results observed in the experiments together with the limit.

4.5 Short-term stability identified a different preferred configuration

Observed result. GCE/PPA/(AmAlg-WO_3)/Ab_{TP} had only 0.92% drift over 45 min, whereas GCE/Ab_{TP} drifted by 4.03%. All configurations changed by no more than 1.38% from 30 to 45 min.

Theories. The involvement of the AmAlg-WO_3 coating in making the hydrated environment created for the mixed recognition layer stable is a hypothesis since the entire data comes from a single measurement and no test was performed with other electrode batches. The plateau level achieved after 30 minutes represented the sampling time but is, in reality, the time of use and not the shelf life.

Relationship to earlier research. Surface chemistry, biomolecule binding, and antifouling or hydrogel matrices can make a difference in the time-dependent behavior of biosensors [7,17]. The present comparison involved obtaining better short-term stability with worse residual calibration results. The choice of a platform should depend on how it is planned to be utilized: for GCE/Ab_{TP}, the emphasis will be on the goodness of calibration fit and LOD based on the model while for GCE/PPA/(AmAlg-WO_3)/Ab_{TP}, it will be on in-session stability.

4.6 Study limitations

Certain limitations must be taken into account. Firstly, the blank dispersions were calculated on the basis of three measurements for each sensor with no further verification of the achieved minimum values compared to the independent standard of low concentrations. Secondly, the calibration tests did not determine the reproducibility of each batch and each sensor. Thirdly, the dataset does not cover selectivity, interference, recoveries, and matrix effects tests. Fourth, the structural characterization has not been performed and thus thickness of PPA, WO_3 distribution, functional group density, and antibody orientation remain undetermined. Fifth, the test series regarding short stability contains one measurement for each time point; the following-day measurement was conducted in the same medium and, therefore, does not allow drawing any conclusions regarding storage stability and shelf life. Finally, conclusions regarding clinical applicability are impossible to make on the basis of buffer calibration only. Evaluation in human serum and comparison with ELISA need to be conducted in a separate paired study.

5. Conclusions

Sequential modification using activated GCE caused observable, but inconsistent changes in HER2 immunosensor performance without any label. PPA was used to provide electropolymerization through the application of ten cycles thus creating a functional coat that prevented the transport of ferri/ferrocyanides and HER2 response. The layer made of AmAlg-WO_3 aided in the partial restoration of both parameters, but the role played by the interface remained different from that of bare GCE. Among the nine systems, GCE/Ab_{TP} provided the best results for the nonlinear calibration and the smallest LOD according to the model, while GCE/PPA/(AmAlg-WO_3)/Ab_{TP} delivered the lowest drift for 45-min duration. Therefore, there is no evidence supporting the presence of the best architecture, but rather, existence of the compromise between the calibration efficiency and the performance stability in the short run, which needs to be investigated in the future.

Data Scope

Everything in this paper is based on the data related to electrode development, the calibration data for HER2, and operational stability data presented in PhD thesis.

References

1. Campuzano, S.; Pedrero, M.; Pingarron, J.M. Non-invasive breast cancer diagnosis through electrochemical biosensing at different molecular levels. Sensors 2017, 17, 1993.

2. Chen, Y.; Qian, C.; Liu, C.; Shen, H.; Wang, Z.; Ping, J.; Wu, J.; Chen, H. The applications of electrochemical immunosensors in the detection of disease biomarkers: A review. Molecules 2023, 28, 3605.

3. Kim, J.; Park, M. Recent progress in electrochemical immunosensors. Biosensors 2021, 11, 360.

4. Emami, M.; Shamsipur, M.; Saber, R.; Irajirad, R. An electrochemical immunosensor for detection of a breast cancer biomarker based on antiHER2-iron oxide nanoparticle bioconjugates. Analyst 2014, 139, 2858–2866.

5. Freitas, M.; Neves, M.M.P.S.; Nouws, H.P.A.; Delerue-Matos, C. Quantum dots as nanolabels for breast cancer biomarker HER2-ECD analysis in human serum. Talanta 2020, 208, 120430.

6. Shamsipur, M.; Emami, M.; Farzin, L.; Saber, R. A sandwich-type electrochemical immunosensor based on in situ silver deposition for determination of serum level of HER2 in breast cancer patients. Biosens. Bioelectron. 2018, 103, 54–61.
7. Wang, W.; Han, R.; Chen, M.; Luo, X. Antifouling peptide hydrogel based electrochemical biosensors for highly sensitive detection of cancer biomarker HER2 in human serum. Anal. Chem. 2021, 93, 7355–7361.
8. Marques, R.C.B.; Viswanathan, S.; Nouws, H.P.A.; Delerue-Matos, C.; Gonzalez-Garcia, M.B. Electrochemical immunosensor for the analysis of the breast cancer biomarker HER2 ECD. Talanta 2014, 129, 594–599.
9. Wignarajah, S.; Chianella, I.; Tothill, I.E. Development of electrochemical immunosensors for HER-1 and HER-2 analysis in serum for breast cancer patients. Biosensors 2023, 13, 355.
10. Al-Hyali, R.H.; Al-Taee, A.T. A new GE/MWCNTs/PFA modified electrode for simultaneous determination of catechol and hydroquinone. Res. J. Pharm. Technol. 2021, 14, 828–832.
11. Al-Taee, A.T.; Al-Hyali, R.H. Electrochemical behavior of oxytocin hormone through its cysteine reduction peak using glassy carbon electrode modified with poly furfurylamine and multi-walled carbon nanotubes. Egypt. J. Chem. 2021, 64, 5831–5837.
12. Al-Taee, A.T.; Al-Layla, A.M.T.; Mahmood, A.R. Electrochemical behavior of aminoguanidine and its detection by hybrid polymer of theophylline with copper oxide nanoparticles. Anal. Bioanal. Electrochem. 2021, 13, 283–295.
13. Felipe, A.C.; do Nascimento, L.A.; Lima, T.M.; Soares, P.I.; Machado, A.R.; Franco, D.L.; Ferreira, L.F.; Brito-Madurro, A.G.; Madurro, J.M. Electropolymerization of p-anisidine: Influence of pH on electrosynthesis. Chem. Pap. 2025, 79, 2091–2104.
14. Nasrollahpour, H.; Naseri, A.; Rashidi, M.-R.; Khalilzadeh, B. Application of green synthesized WO3-poly(glutamic acid) nanobiocomposite for early-stage biosensing of breast cancer using an electrochemical approach. Sci. Rep. 2021, 11, 23994.
15. Cho, H.-S.; Mason, K.; Ramyar, K.X.; Stanley, A.M.; Gabelli, S.B.; Denney, D.W., Jr.; Leahy, D.J. Structure of the extracellular region of HER2 alone and in complex with the Herceptin Fab. Nature 2003, 421, 756–760.
16. Franklin, M.C.; Carey, K.D.; Vajdos, F.F.; Leahy, D.J.; de Vos, A.M.; Sliwkowski, M.X. Insights into ErbB signaling from the structure of the ErbB2-pertuzumab complex. Cancer Cell 2004, 5, 317–328.
17. Gao, S.; Guisan, J.M.; Rocha-Martin, J. Oriented immobilization of antibodies onto sensing platforms: A critical review. Anal. Chim. Acta 2022, 1189, 338907.
18. Patel, M.; Agrawal, M.; Srivastava, A. Signal amplification strategies in electrochemical biosensors via antibody immobilization and nanomaterial-based transducers. Mater. Adv. 2022, 3, 8864–8885.